Activation Timing Control Using On-board Camera for Dynamic Wireless Power Transfer Under Circuit Parameter Variations

Ryo Matsumoto [1)] **Hiroshi Fujimoto** [1)]

1) Graduate School of Frontier Sciences, The University of Tokyo, Kashiwa, Chiba, Japan

E-mail: matsumoto.ryo19@ae.k.u-tokyo.ac.jp

ABSTRACT: This paper proposes an activation timing control method for dynamic wireless power transfer systems using an on-board depth camera. Conventional timing control methods have used the electrical information of the circuit to detect the approaching vehicle. However, these methods cannot maintain their performance when the parameters of the circuit vary from their designed values. The method proposed in this paper avoids this problem by using the visual information obtained by the depth camera to determine the activation timing. The experimental results demonstrate that the proposed method can maintain a consistent activation timing when the self-inductance of the transmitter and receiver coils vary from their designed values.

KEY WORDS: electric vehicle, wireless power transfer, vehicle detection, mistuning, image processing

1. INTRODUCTION

Electric vehicles (EVs) have several major disadvantages compared to conventional petrol vehicles such as short cruising range, long charging time, and expensive batteries. An emerging technology called dynamic wireless power transfer (DWPT) is considered as a potential solution to these issues[(1)(2)]. Electric power is transmitted wirelessly from the transmitter (Tx) coil embedded in the road to the receiver (Rx) coil attached to the vehicle chassis, while the vehicle is in motion.

One of the key challenges of this technology is the precise timing control of the power transfer process. If the power transfer is activated when the vehicle is not directly above the Tx coil, an excessively large current flows through the Tx coil which damages the circuit components and emits a strong electromagnetic field[(3)]. Moreover, the vehicle cannot receive the desired amount of power from the road if the activation timing is too late or too early.

Several studies[(4)(5)] have proposed methods using additional coils and sensors to detect the approaching vehicle and determine the activation timing. However, the additional coils and sensors increase the cost of the system and entail the risk of malfunction or failure. Other studies[(6)-(8)] have proposed methods to estimate the position of the vehicle from the road side using the electrical information of the WPT circuit. In (6), sharp voltage pulses are applied to the Tx circuit, and the approaching vehicle is detected by monitoring the amplitude of the Tx coil current. The methods in (6)-(8) depend on the accuracy of the WPT circuit model. However, in practical DWPT applications, the parameters of circuit components can vary from their designed values, making the WPT circuit model inaccurate. For example, the manufacturing tolerance and aging of the coils and compensation capacitors are inevitable. Moreover, the self-inductance of the Tx and Rx coils varies depending on the position of the Rx coil, since the coils are usually equipped with ferrite blocks and aluminum shields[(9)]. These parameter variations can affect the activation timing of the power transfer.

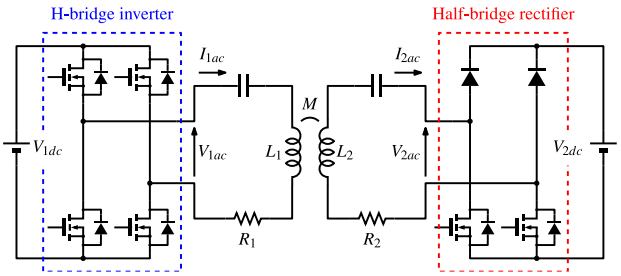

Fig. 1 Equivalent circuit model of the DWPT system.

In recent years, advanced driver assistance systems (ADAS) such as lane keeping assist and adaptive cruise control are developing and being introduced into commercial vehicles[(10)(11)]. The image information and distance information obtained by cameras, LiDARs, and radars play an important role in these technologies[(12)(13)]. If ADAS continues to spread, most commercial vehicles will be equipped with cameras and distance measuring devices in the near future.

This paper proposes an activation timing control method using the information of the depth camera mounted on the vehicle. The proposed method is robust against circuit parameter variations since it does not rely on the electrical information of the WPT

Copyright © 2023 Society of Automotive Engineers of Japan, Inc.

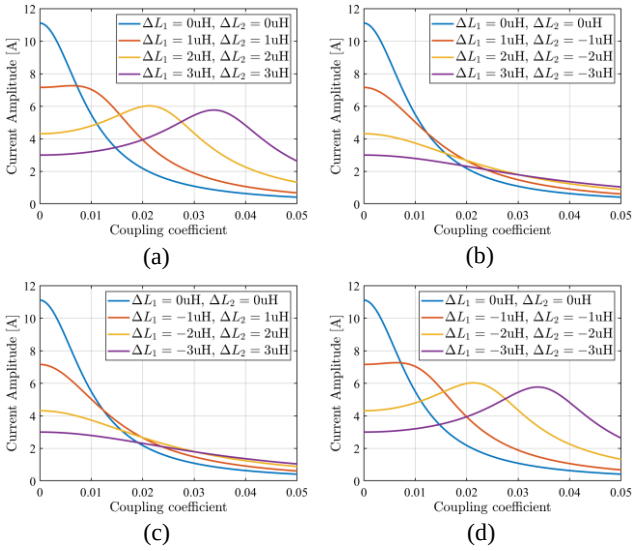

Fig. 2 Amplitude of the Tx coil current as a function of the coupling coefficient under diverse patterns of self-inductance variations. (a) $\Delta L_1 \geq 0$, $\Delta L_2 \geq 0$. (b) $\Delta L_1 \geq 0$, $\Delta L_2 \leq 0$. (c) $\Delta L_1 \leq 0$, $\Delta L_2 \geq 0$. (d) $\Delta L_1 \leq 0$, $\Delta L_2 \leq 0$.

circuit. Moreover, the proposed method does not require additional coils and sensors besides the depth camera. Since the depth camera is mainly used for driver assistance purposes, no additional cost is introduced by the proposed activation timing control method.

2. ANALYSIS OF THE CONVENTIONAL METHOD CONSIDERING CIRCUIT PARAMETER VARIATIONS

Fig. 1 shows the equivalent circuit model of the DWPT system. L_1, L_2, and M represent the self-inductance of the Tx coil, the self-inductance of the Rx coil, and the mutual inductance. C_1 and C_2 represent the capacitance of the compensation capacitors. R_1 and R_2 represent the equivalent series resistance (ESR) of the Tx and Rx circuits. The values of L_1, L_2, C_1 and C_2 are designed based on the resonant condition:

$$\omega = \frac{1}{\sqrt{L_1 C_1}} = \frac{1}{\sqrt{L_2 C_2}} \tag{1}$$

where ω is the operating angular frequency of the inverter. The coupling coefficient between the Tx and Rx coils is defined as:

$$k = \frac{M}{\sqrt{L_1 L_2}}. \tag{2}$$

The principles of the vehicle detection method proposed in [6] are as follows. When the vehicle is approaching the Tx coil, the duty cycle of the inverter is set to a small value to generate sharp voltage pulses. The MOSFETs of the half-bridge rectifier are both turned ON to create a short circuit. Under these conditions, the amplitude of the Tx coil current can be expressed as:

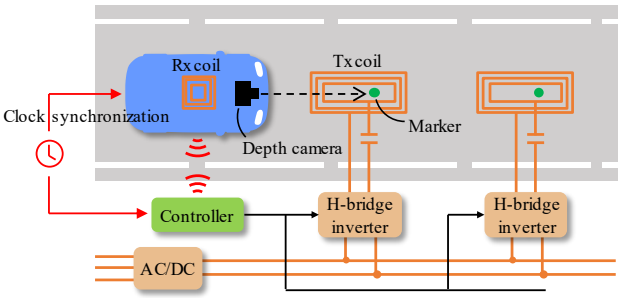

Fig. 3 Overview of the proposed activation timing control.

$$I_{1ac} = \frac{R_2}{R_1 R_2 + (\omega M)^2} V_{1ac}. \tag{3}$$

From (3), when $R_1 R_2$ is sufficiently small compared to $(\omega M)^2$, the amplitude of the Tx coil current decreases as the coupling coefficient increases. When the amplitude of the Tx coil current falls below a pre-determined threshold, the system assumes that the vehicle is close enough to the Tx coil and activates the power transfer process.

When the self-inductance of the Tx and Rx coils vary from their designed values, the amplitude of the Tx coil current can be expressed as:

$$I_{1ac} = \frac{V_{1ac}}{\sqrt{A^2 + B^2}} \tag{4}$$

where

$$A \coloneqq R_1 + \frac{(\omega M)^2}{R_2^2 + (\omega \Delta L_2)^2} R_2 \tag{5}$$

$$B \coloneqq \Delta L_1 - \frac{(\omega M)^2}{R_2^2 + (\omega \Delta L_2)^2} \Delta L_2. \tag{6}$$

ΔL_1 and ΔL_2 represent the self-inductance variations of the Tx and Rx coils. Based on equations (4)-(6), the amplitude of the Tx coil current as a function of the coupling coefficient under diverse self-inductance variations can be obtained as shown in Fig. 2. The parameters used in the calculation are the same as the experimental setup in Section 4. As can be seen from Fig. 2, the behavior of the Tx coil current changes when the self-inductance of the coils varies from their designed values. In fact, if the power transfer is activated when the amplitude of the Tx coil current falls below a pre-determined threshold, the activation timing is likely to change depending on the self-inductance variations of the Tx and Rx coils.

3. ACTIVATION TIMING CONTROL USING ON-BOARD DEPTH CAMERA

Fig. 3 shows the overview of the proposed activation timing control method. A visual marker is embeddd on the road surface to indicate the position of the Tx coil. A depth camera is mounted on the vehicle to measure the spatial distance to the marker. In this

Copyright © 2023 Society of Automotive Engineers of Japan, Inc.

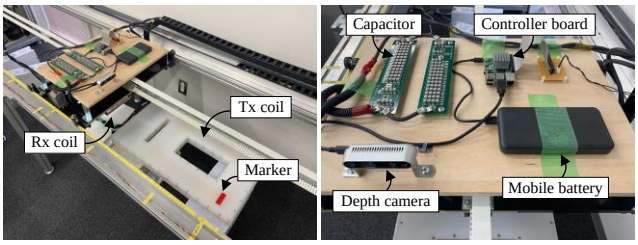

Fig. 4 Experimental setup of the DWPT test bench.

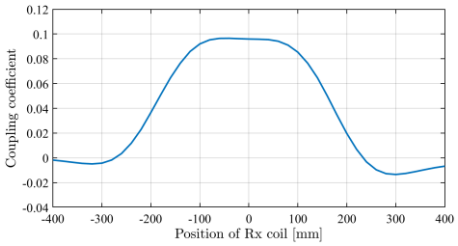

Fig. 5 Coupling coefficient as a function of the Rx coil position.

paper, it is assumed that the position of the vehicle is kept in the center of the lane by automated steering. Also, the velocity of the vehicle is assumed to be constant for simplicity. The horizontal distance from the camera to the marker can be expressed as:

$$d[i] = \sqrt{l[i]^2 - h^2} \tag{7}$$

where l represents the spatial distance to the marker, and h represents the vertical distance of the camera from the ground. The variation in h caused by the suspension is neglected since it has only minor negative effects when l is sufficiently larger than h. $d[i]$ and $l[i]$ represent the i-th sample of d and l. The time of arrival to the activation point can be calculated as:

$$t_{act}[i] = t[i] + \frac{d[i] - d_{marker}}{v} \tag{8}$$

where $t[i]$ represents the time when $l[i]$ is obtained, d_{marker} represents the distance between the activation point and the marker, and v represents the velocity of the vehicle. The measurement error of the depth camera can be reduced by taking the average of k samples as:

$$\overline{t_{act}} = \frac{1}{k}(t_{act}[0] + t_{act}[1] + \cdots + t_{act}[k-1]). \tag{9}$$

The above calculation can be fully conducted on the vehicle side. However, since the activation timing is controlled by the H-bridge inverter, the information of $\overline{t_{act}}$ is required on the road side. This can be solved by applying clock synchronization *e.g.* Precision Time Protocol (PTP)[14] between the vehicle side and the road side controller and exchanging the information of $\overline{t_{act}}$ through wireless communication. PTP can achieve clock accuracy in the order of microseconds. Considering that it takes tens to hundreds of milliseconds for a vehicle to pass over a single Tx coil[1], the accuracy of PTP is sufficiently high for DWPT applications. After activating the inverter at $\overline{t_{act}}$, the inverter is deactivated at t_{deact} which is given by:

$$t_{deact} = \overline{t_{act}} + \frac{d_{deact}}{v} \tag{10}$$

where d_{deact} represents the distance between the activation point and the deactivation point. Since the above method does not rely on the electrical information of the WPT circuit, the activation and deactivation timing will not be affected by circuit parameter variations.

Table Ⅰ Specifications of the experimental setup.

Operating frequency	85 kHz
Tx side DC voltage, V_{1dc}	50 V
Rx side DC voltage, V_{2dc}	50 V
Self-inductance of Tx coil, L_1	134.7 μH
Self-inductance of Rx coil, L_2	53.9 μH
Tx side compensation capacitance, C_1	25.9 nF
Rx side compensation capacitance, C_2	65.2 nF
ESR of Tx circuit, R_1	136 mΩ
ESR of Rx circuit, R_2	108 mΩ
Velocity of Rx coil	0.3 km/h

4. EXPERIMENTAL VERIFICATION

An experimental comparison of the conventional and proposed method is conducted on the DWPT test bench shown in Fig. 4. The specifications of the experimental setup are listed in Table Ⅰ. In the experiment, four cases of self-inductance variations *i.e.* $(\Delta L_1, \Delta L_2) = (0\mu H, 0\mu H), (1\mu H, 1\mu H), (2\mu H, 2\mu H), (3\mu H, 3\mu H)$ are studied. Instead of directly changing the inductance of the coils, additional coils are connected in series to the Tx and Rx coils to emulate the self-inductance variations. The coupling coefficient between the Tx and Rx coils is shown in Fig. 5. The velocity of the Rx coil is controlled to 0.3 km/h by a servo motor. In the conventional method, the power transfer is activated when I_{1ac} falls below 3 A during the detection phase, and the power transfer is deactivated when I_{1ac} exceeds 25 A during the transmission phase. In the proposed method, a depth camera is mounted on the moving part of the test bench. When the Rx coil reaches the activation point, a signal is sent from the Rx side controller to the Tx side controller by wired communication.

Figs. 6 and 7 show the waveforms of the conventional method during the detection phase and the transmission phase, respectively. The waveforms are obtained under $(\Delta L_1, \Delta L_2) = (0\mu H, 0\mu H)$. As shown in Fig. 6, sharp voltage pulses are applied to the Tx circuit at intervals of 0.5 ms. If the amplitude of I_{1ac}

Copyright © 2023 Society of Automotive Engineers of Japan, Inc.

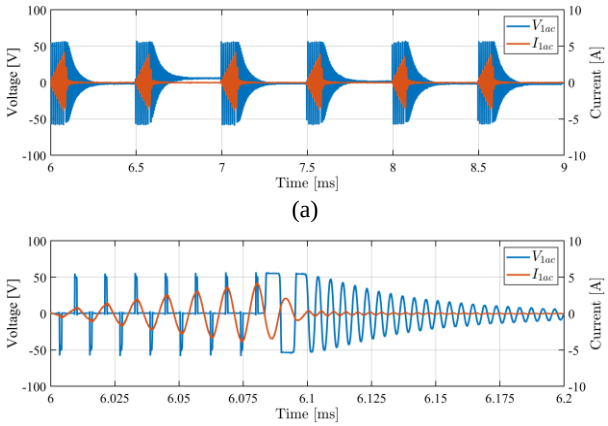

Fig. 6 Waveforms of the conventional method during the detection phase. (a) Waveforms of V_{1ac} and I_{1ac}. (b) Scaled-up waveforms of V_{1ac} and I_{1ac}.

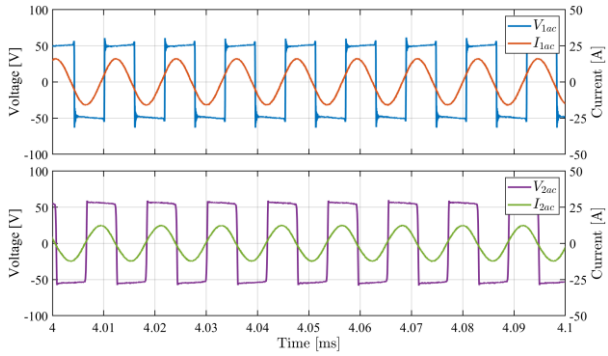

Fig. 7 Waveforms of the conventional method during the transmission phase.

exceeds 3 A, the voltage pulses are turned off. If the amplitude of I_{1ac} does not exceed 3 A for 0.5 ms, the Tx side controller assumes that the Rx coil is close enough and moves on to the transmission phase. Fig. 8 shows the scaled-down waveforms of the conventional method under the four cases of self-inductance variations. It can be seen from Fig. 8 that the activation timing is delayed when the self-inductance of the Tx and Rx coils increase from their designed values. The reason for this is that the behavior of the Tx coil current during the detection phase changes when the self-inductance of the coils vary, as discussed in Section 2. The delay in the activation timing means that the vehicle cannot receive the maximum available energy when passing over a single Tx coil.

Fig. 9 shows the color images and depth maps obtained by the camera at two different positions of the Rx coil. In the experiment, the marker is recognized based on the RGB values of the color image. Fig. 10 shows the horizontal distance between the camera and the marker calculated by the Rx side controller when moving the Rx coil at 0.3 km/h. The relationship between the calculated horizontal distance and the time is nearly linear, indicating that the

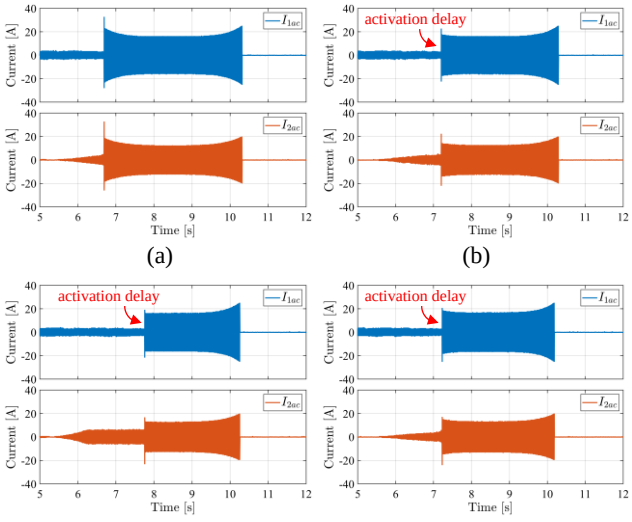

Fig. 8 Waveforms of the conventional method under the four cases of self-inductance variations. (a) $\Delta L_1 = 0\mu\text{H}$, $\Delta L_2 = 0\mu\text{H}$. (b) $\Delta L_1 = 1\mu\text{H}$, $\Delta L_2 = 1\mu\text{H}$. (c) $\Delta L_1 = 2\mu\text{H}$, $\Delta L_2 = 2\mu\text{H}$. (d) $\Delta L_1 = 3\mu\text{H}$, $\Delta L_2 = 3\mu\text{H}$.

distance to the marker is successfully being measured by the depth camera.

Fig. 11 shows the scaled-down waveforms of the proposed method under the four cases of self-inductance variations. It can be seen from Fig. 11 that the activation timing is roughly the same among the four cases. The activation timing does not depend on the self-inductance variations since the proposed method is based on the visual information obtained by the depth camera.

Table Ⅱ gives a comparison of the conventional and proposed methods in terms of the delay of the activation timing. The delay is measured with respect to the activation timing of the conventional method under $(\Delta L_1, \Delta L_2) = (0\mu\text{H}, 0\mu\text{H})$. In the proposed method, the activation timing was not exactly consistent every trial due to the measurement error of the depth camera. Therefore, Table Ⅱ lists the minimum, maximum, and mean delay of 5 trials. The activation timing is delayed by more than 0.5 s when the conventional method is applied under self-inductance variations. On the other hand, the activation timing is delayed by no more than 0.07 s when the proposed method is applied. These results verify that the proposed method can maintain a consistent activation timing under the self-inductance variations of the coils.

4. CONCLUSION

This paper proposed an activation timing control method for DWPT using a depth camera on the vehicle. Compared to the conventional method using the electrical information of the circuit, the proposed method can maintain a consistent activation timing when the self-inductance of the Tx and Rx coils vary from their

Copyright © 2023 Society of Automotive Engineers of Japan, Inc.

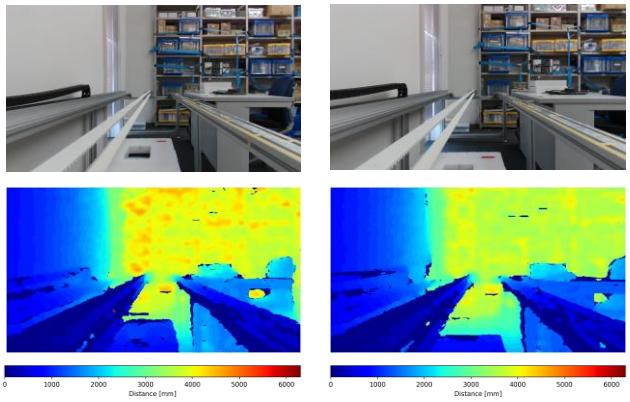

(a) (b)

Fig. 9 Color image and depth map obtained by the camera at (a) $d = 1200$ mm and (b) $d = 900$ mm.

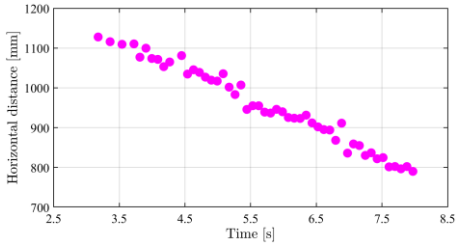

Fig. 10 Horizontal distance to the marker measured by the depth camera.

designed values. By applying the proposed method, the power transfer process can be activated without delay, thus providing the maximum available energy to the vehicle.

In the experiment conducted in this paper, the velocity of the Rx coil was set to a very slow speed to validate the basic concept of the proposed method. However, in practical DWPT applications, the velocity of the vehicle is much faster and can exceed 100 km/h in highway applications. In these conditions, the accuracy of the proposed method will depend on the sampling period of the depth camera and the processing speed of the Rx side controller. In addition, the communication delay between the Tx and Rx side controllers must be considered. The improvement of the proposed method taking these aspects into account will be addressed in future works.

ACKNOWLEDGEMENT

This work was partly supported by JST SPRING Grant Number JPMJSP2108, JST-Mirai Program Grant Number JPMJMI21E2, JSPS KAKENHI Grant Number JP18H03768 and project JPNP21005 subsidized by the New Energy and Industrial Technology Development Organization (NEDO).

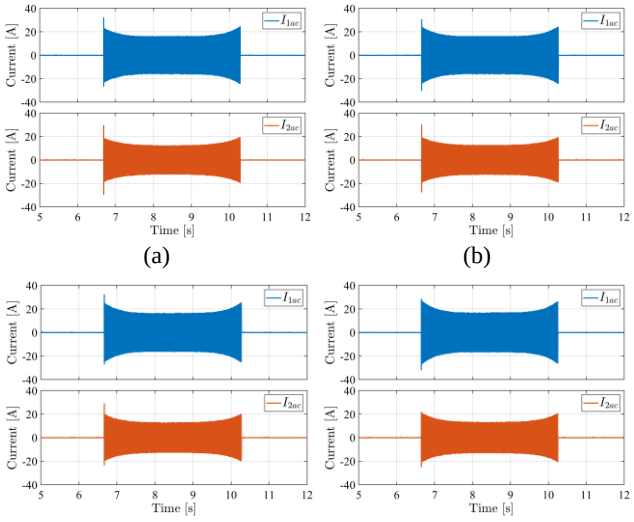

(a) (b)

(c) (d)

Fig. 11 Waveforms of the proposed method under the four cases of self-inductance variations. (a) $\Delta L_1 = 0\mu\text{H}$, $\Delta L_2 = 0\mu\text{H}$. (b) $\Delta L_1 = 1\mu\text{H}$, $\Delta L_2 = 1\mu\text{H}$. (c) $\Delta L_1 = 2\mu\text{H}$, $\Delta L_2 = 2\mu\text{H}$. (d) $\Delta L_1 = 3\mu\text{H}$, $\Delta L_2 = 3\mu\text{H}$.

Table Ⅱ Delay in the activation timing.

	Conv.	Prop. (Result of 5 trials)		
		Min.	Max.	Mean
$\Delta L_1 = 0\mu\text{H}$ $\Delta L_2 = 0\mu\text{H}$	0.00 s (baseline)	-0.11 s	0.05 s	0.00 s
$\Delta L_1 = 1\mu\text{H}$ $\Delta L_2 = 1\mu\text{H}$	0.51 s	-0.03 s	0.06 s	0.00 s
$\Delta L_1 = 2\mu\text{H}$ $\Delta L_2 = 2\mu\text{H}$	1.07 s	-0.03 s	0.06 s	0.00 s
$\Delta L_1 = 3\mu\text{H}$ $\Delta L_2 = 3\mu\text{H}$	0.54 s	-0.06 s	0.07 s	0.01 s

REFERENCES

(1) V. Cirimele et al., "The Fabric ICT Platform for Managing Wireless Dynamic Charging Road Lanes," in IEEE Transactions on Vehicular Technology, vol. 69, no. 3, pp. 2501-2512, March 2020.

(2) A. C. Bagchi, A. Kamineni, R. A. Zane and R. Carlson, "Review and Comparative Analysis of Topologies and Control Methods in Dynamic Wireless Charging of Electric Vehicles," in IEEE Journal of Emerging and Selected Topics in Power Electronics, vol. 9, no. 4, pp. 4947-4962, Aug. 2021.

(3) K. Kusaka, R. Kusui, J. Itoh, D. Sato, T. Shijo, S. Obayashi and M. Ishida, "A 22kW Three-phase Wireless Power Transfer System in Compliance with CISPR 11 and ICNIRP 2010, " in IEEJ Transactions on Industry Applications, vol. 11, no. 4, pp. 594-602, 2022.

Copyright © 2023 Society of Automotive Engineers of Japan, Inc.

(4) X. Zhang, W. Zhang, Y. Zheng and X. Fan, "Research on Dynamic Wireless Charging Control Strategy of Electric Vehicle Based on Photoelectric Detection and Location," 2019 12th International Symposium on Computational Intelligence and Design (ISCID), Hangzhou, China, 2019, pp. 266-269.

(5) D. Patil, J. M. Miller, B. Fahimi, P. T. Balsara and V. Galigekere, "A Coil Detection System for Dynamic Wireless Charging of Electric Vehicle," in IEEE Transactions on Transportation Electrification, vol. 5, no. 4, pp. 988-1003, Dec. 2019.

(6) D. Kobayashi, K. Hata, T. Imura, H. Fujimoto and Y. Hori, "Sensorless Vehicle Detection Using Voltage Pulses in Dynamic Wireless Power Transfer System, " EVS29 Symposium, Jun. 2016.

(7) D. Shirasaki, H. Fujimoto and Y. Hori, "Sensorless Vehicle Detection Using Vehicle Side Voltage Pulses for In-motion WPT," 2020 IEEE PELS Workshop on Emerging Technologies: Wireless Power Transfer (WoW), Seoul, Korea (South), 2020, pp. 320-325.

(8) Akihiro Okazaki, Takehiro Imura, Yoichi Hori, "Transmission Circuit Switching Control System Combining Speed Estimation and N-Legged Converter for Dynamic Wireless Power Transfer", 2022 Asian Wireless Power Transfer Workshop (AWPT2022), Dec. 2022.

(9) M. Maemura, T. Kurpat, K. Kimura, T. Suzuki and T. Hashimoto, "Improvement of the Power Transfer Efficiency of a Dynamic Wireless Power Transfer System via Spatially Distributed Soft Magnetic Materials," 2022 Wireless Power Week (WPW), Bordeaux, France, 2022, pp. 332-337.

(10) Q. Zou, H. Jiang, Q. Dai, Y. Yue, L. Chen and Q. Wang, "Robust Lane Detection From Continuous Driving Scenes Using Deep Neural Networks," in IEEE Transactions on Vehicular Technology, vol. 69, no. 1, pp. 41-54, Jan. 2020.

(11) M. Hattori, O. Shimizu, S. Nagai, H. Fujimoto, K. Sato, Y. Takeda and T. Nagashio, "Quadrant Dynamic Programming for Optimizing Velocity of Ecological Adaptive Cruise Control," in IEEE/ASME Transactions on Mechatronics, vol. 27, no. 3, pp. 1533-1544, June 2022.

(12) X. Chen, H. Ma, J. Wan, B. Li and T. Xia, "Multi-view 3D Object Detection Network for Autonomous Driving," 2017 IEEE Conference on Computer Vision and Pattern Recognition (CVPR), Honolulu, HI, USA, 2017, pp. 6526-6534.

(13) S. Sun, A. P. Petropulu and H. V. Poor, "MIMO Radar for Advanced Driver-Assistance Systems and Autonomous Driving: Advantages and Challenges," in IEEE Signal Processing Magazine, vol. 37, no. 4, pp. 98-117, July 2020.

(14) "IEC/IEEE International Standard - Precision Clock Synchronization Protocol for Networked Measurement and Control Systems," in IEC/IEEE 61588-2021 , vol., no., pp.1-504, 8 June 2021.

Copyright © 2023 Society of Automotive Engineers of Japan, Inc.